

Catalytic Mechanism and Three-Dimensional Structure of Adenine Deaminase^{†,‡}

Siddhesh S. Kamat,[§] Ashima Bagaria,^{||} Desigan Kumaran,^{||} Gregory P. Holmes-Hampton,[§] Hao Fan,[@] Andrej Sali,[@] J. Michael Sauder,[†] Stephen K. Burley,[†] Paul A. Lindahl,[§] Subramanyam Swaminathan,^{*,||} and Frank M. Raushel^{*,§}

[§]Department of Chemistry, P.O. Box 30012, Texas A&M University, College Station, Texas 77843-3012, United States, ^{||}Biology Department, Brookhaven National Laboratory, P.O. Box 5000, Upton, New York 11973-5000, United States, [†]Eli Lilly and Company, Lilly Biotechnology Center, 10300 Campus Point Drive, Suite 200, San Diego, California 92121, United States, and [@]Department of Bioengineering and Therapeutic Sciences and Department of Pharmaceutical Chemistry, California Institute for Quantitative Biosciences, University of California, San Francisco, 1700 4th Street, San Francisco, California 94158, United States

Received November 8, 2010; Revised Manuscript Received January 18, 2011

ABSTRACT: Adenine deaminase (ADE) catalyzes the conversion of adenine to hypoxanthine and ammonia. The enzyme isolated from *Escherichia coli* using standard expression conditions was low for the deamination of adenine ($k_{\text{cat}} = 2.0 \text{ s}^{-1}$; $k_{\text{cat}}/K_{\text{m}} = 2.5 \times 10^3 \text{ M}^{-1} \text{ s}^{-1}$). However, when iron was sequestered with a metal chelator and the growth medium was supplemented with Mn^{2+} prior to induction, the purified enzyme was substantially more active for the deamination of adenine with k_{cat} and $k_{\text{cat}}/K_{\text{m}}$ values of 200 s^{-1} and $5 \times 10^5 \text{ M}^{-1} \text{ s}^{-1}$, respectively. The apoenzyme was prepared and reconstituted with Fe^{2+} , Zn^{2+} , or Mn^{2+} . In each case, two enzyme equivalents of metal were necessary for reconstitution of the deaminase activity. This work provides the first example of any member of the deaminase subfamily of the amidohydrolase superfamily to utilize a binuclear metal center for the catalysis of a deamination reaction. $[\text{Fe}^{\text{II}}/\text{Fe}^{\text{II}}]$ -ADE was oxidized to $[\text{Fe}^{\text{III}}/\text{Fe}^{\text{III}}]$ -ADE with ferricyanide with inactivation of the deaminase activity. Reducing $[\text{Fe}^{\text{III}}/\text{Fe}^{\text{III}}]$ -ADE with dithionite restored the deaminase activity, and thus, the diferrous form of the enzyme is essential for catalytic activity. No evidence of spin coupling between metal ions was evident by electron paramagnetic resonance or Mössbauer spectroscopy. The three-dimensional structure of adenine deaminase from *Agrobacterium tumefaciens* (Atu4426) was determined by X-ray crystallography at 2.2 Å resolution, and adenine was modeled into the active site on the basis of homology to other members of the amidohydrolase superfamily. On the basis of the model of the adenine–ADE complex and subsequent mutagenesis experiments, the roles for each of the highly conserved residues were proposed. Solvent isotope effects, pH–rate profiles, and solvent viscosity were utilized to propose a chemical reaction mechanism and the identity of the rate-limiting steps.

Adenine deaminase (ADE)¹ catalyzes the conversion of adenine to hypoxanthine and ammonia as shown in Scheme 1 (1, 2). ADE is part of the purine degradation pathway in which hypoxanthine is subsequently oxidized to uric acid by xanthine oxidase via a xanthine intermediate (3). This enzyme also participates in the purine salvage pathway for the synthesis of guanine nucleotides (1). ADE from *Escherichia coli* is a member of the amidohydrolase superfamily (AHS) and is clustered within cog1001 in the NCBI database (4, 5). Enzymes capable of deaminating adenosine, guanine, cytosine, and *S*-adenosylhomocysteine (SAH) are also found within the AHS. All structurally characterized deaminases in the AHS have a distorted (β/α)₈-barrel structural fold and have a single divalent cation in the active site that is utilized for the activation of the nucleophilic water molecule (5). For these enzymes, the lone divalent metal ion

is coordinated to two histidines at the end of β -strand 1, another histidine at the end of β -strand 5, an aspartate at the end of β -strand 8, and a water molecule. A triad of conserved active site residues catalyzes transfers of protons from the metal-ligated water molecule to the reaction products, ammonia and hypoxanthine (5–7). These three residues include a glutamate in the loop that follows β -strand 5 (HxxE motif), a histidine at the C-terminal end of β -strand 6, and the aspartate at the C-terminus of β -strand 8.

On the basis of amino acid sequence alignments, the putative adenine deaminases found within cog1001 are predicted to bind two divalent cations in the active site to form a binuclear metal center structurally similar to those found in phosphotriesterase (8, 9), urease (10), and iso-aspartyl dipeptidase (11, 12). In the known adenine deaminases from cog1001, there are four invariant histidine residues at the C-terminal ends of β -strands 1, 5, and 6 and an aspartate at the C-terminus of β -strand 8. A conserved glutamate residue that resides at the end of β -strand 4 is positioned to bridge the two divalent cations. For *E. coli* ADE, these residues are predicted to be His-90, His-92, Glu-185, His-214, His-235, and Asp-284. Adenine deaminase does not have the signature HxxE motif at the end of β -strand 5 that is conserved in all of the other known deaminases in the amidohydrolase superfamily (5). Therefore, the mechanism for the deamination of

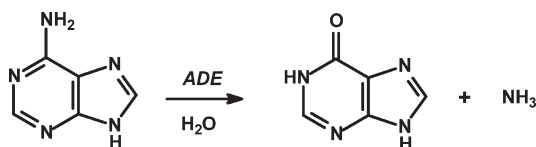
[†]This work was supported in part by the National Institutes of Health (Grants GM 71790, GM074945, and GM 46441).

[‡]The X-ray coordinates and structure factors for Atu4426 have been deposited in the Protein Data Bank as entry 3nqb.

*To whom correspondence should be addressed. F.M.R.: telephone, (979) 845-3373; fax, (979) 845-9452; e-mail, raushel@tamu.edu. S.S.: telephone, (631) 344-3187; fax, (631) 344-3407; e-mail, swami@bnl.gov.

Abbreviations: ADE, adenine deaminase; IPTG, isopropyl β -thiogalactoside; AHS, amidohydrolase superfamily; ICP-MS, inductively coupled plasma mass spectrometry; GDH, glutamate dehydrogenase; rmsd, root-mean-square deviation.

Scheme 1



adenine by ADE is expected to be somewhat different from those of the reactions catalyzed by adenosine, cytosine, and guanine deaminases.

Previous attempts to isolate and characterize ADE from *E. coli* using standard expression and purification protocols have shown that slightly more active enzyme could be obtained when the growth medium was supplemented with Mn^{2+} (1, 2). However, the specific activity of the purified enzyme was substantially lower when compared with the turnover numbers exhibited by other deaminases from the amidohydrolase superfamily (1, 2). The turnover number for the deamination of adenine by ADE from *E. coli* was approximately 2 s^{-1} and the enzyme isolated with a mixture of zinc, manganese, and iron in the active site. Here we present a novel iron-free expression and purification protocol resulting in the isolation of adenine deaminase with a turnover number of approximately 200 s^{-1} . We determined the three-dimensional structure of ADE from *Agrobacterium tumefaciens* (Atu4426) and proposed a novel catalytic reaction mechanism for the deamination of adenine.²

MATERIALS AND METHODS

Materials. All chemicals were purchased from Sigma-Aldrich unless otherwise stated. The genomic DNA for *E. coli* K12 was purchased from ATCC. *E. coli* BL21(DE3) and XL1-blue competent cells were obtained from Stratagene. Expression vector pET30(+) and Pfx DNA polymerase were purchased from Invitrogen. All oligonucleotides were obtained from the Gene Technology Lab at Texas A&M University.

Cloning of Adenine Deaminase from *E. coli*. The DNA sequence for adenine deaminase from *E. coli* K12 was cloned (gi|16131535). The PCR product was amplified utilizing the primer pair 5'-AGGCTATTAATGAATAATTCTATTAACCATAA-ATTCATCAT-3' and 5'-CCGGAATTCTTATTCGGT-GACTTCCAGCGTAGTGAAG-3'. *AseI* and *EcoRI* restriction sites were introduced into the forward and reverse primers, respectively. The PCR product was purified with a PCR cleanup system (Promega), digested with *AseI* and *EcoRI*, and ligated into a pET30a(+) vector that was previously digested with *AseI* and *EcoRI*. The cloned gene fragment was sequenced to verify the fidelity of the PCR amplification.

Standard Protein Expression and Purification of *E. coli* ADE. The recombinant plasmid bearing the gene for adenine deaminase was transformed into *E. coli* BL21(DE3) competent cells by electroporation. A single colony was grown overnight at 37 °C in 5 mL of LB medium containing 50 $\mu\text{g}/\text{mL}$ kanamycin. Aliquots (5 mL) were used to inoculate 6 L of the same medium. The cell cultures were grown at 37 °C and induced with 0.5 mM isopropyl β -thiogalactoside (IPTG) when the A_{600} reached ~ 0.6 in the presence of 1.0 mM MnCl_2 . Protein expression was confirmed by sodium dodecyl sulfate–polyacrylamide gel electrophoresis.

The cells were centrifuged and then resuspended in 50 mM HEPES (pH 7.5) containing 0.1 mg/mL phenylmethanesulfonyl fluoride and lysed by sonication. The soluble proteins were separated from the cell debris by centrifugation at 12000g for 15 min at 4 °C. The nucleic acids were removed by dropwise addition of 2% (w/v) protamine sulfate. After centrifugation, solid ammonium sulfate was added to 60% saturation to the supernatant solution. The precipitated protein was dissolved in buffer and then applied to a High Load 26/60 Superdex 200 prep grade gel filtration column (GE Healthcare). The active fractions were pooled and loaded onto a ResourceQ column (6 mL) and eluted with a gradient of NaCl in 20 mM HEPES (pH 7.5).

Iron-Free Protein Expression of *E. coli* ADE. The iron content of our LB medium was determined to be approximately 36 μM by inductively coupled plasma mass spectrometry (ICP-MS). The iron-specific chelator 2,2'-dipyridyl was used to remove this metal during protein expression. A single colony was grown overnight at 37 °C in 5 mL of LB medium containing 50 $\mu\text{g}/\text{mL}$ kanamycin and then added to 6 L of the same medium. When the A_{600} reached 0.15–0.20, 50 μM 2,2'-dipyridyl was added to sequester the iron, followed by the addition of 0.5 mM IPTG and 1.0 mM MnCl_2 when the A_{600} was ~ 0.6 .

Cloning, Expression, and Purification of Atu4426. The gene for adenine deaminase (gi|15890557) was obtained from *A. tumefaciens* genomic DNA (ATCC 33970D) and cloned into a custom TOPO-isomerase vector, pSGX3(BC), supplied by Invitrogen. Forward and reverse primers were ACCGCGCA-AATCCGCTGGCGGAGC and CTCCAAAACCTCGA-TGACCGGGCTTTCC, respectively. The clone encodes Met-Ser-Leu followed by the PCR product and Glu-Gly-His₆. Miniprep DNA was transformed into BL21(DE3)-Codon+RIL expression cells (Stratagene), expressed, and made into a 30% glycerol stock for large-scale fermentation. The Atu4426 expression clone was cultured using High Yield selenomethionine (SeMet) medium (Orion Enterprises, Inc., Northbrook, IL); 50 mL overnight cultures in 250 mL baffled flasks were cultivated at 37 °C from a frozen glycerol stock for 16 h. Overnight cultures were then transferred to 2 L baffled shake flasks containing 1 L of High Yield SeMet medium (100 $\mu\text{g}/\text{mL}$ kanamycin and 30 $\mu\text{g}/\text{mL}$ chloramphenicol) and grown to an OD_{600} of 1.0–1.2. SeMet was then added for labeling at 120 mg/L, followed by IPTG added to a final concentration of 0.4 mM. In addition, 70 μM MnCl_2 and 100 μM 2,2'-dipyridyl (final concentrations) were added prior to expression to remove iron and prevent side chain modifications. Cells were further grown at 22 °C for 18 h, then harvested using standard centrifugation for 10 min at 6000 rpm, and frozen at -80 °C.

Cells were lysed in 20 mM Tris (pH 8.0), 0.5 M NaCl, 25 mM imidazole, and 0.1% Tween 20 by sonication. The cellular debris was removed by centrifugation for 30 min (39800g). The supernatant was collected and incubated with 10 mL of a 50% slurry of Ni-NTA agarose (Qiagen) for 30 min with gentle stirring. The sample was then poured into a drip column and washed with 50 mL of wash buffer [20 mM Tris-HCl (pH 8.0), 500 mM NaCl, 10% glycerol, and 25 mM imidazole] to remove unbound proteins. The protein of interest was eluted using 25 mL of elution buffer (wash buffer with 500 mM imidazole). Fractions containing the protein were pooled and further purified by gel filtration chromatography on a GE Healthcare HiLoad 16/60 Superdex 200 prep grade column preequilibrated with gel filtration buffer [10 mM HEPES (pH 7.5), 150 mM NaCl, 10% glycerol, and 5 mM DTT]. Fractions containing the protein of

²In the Protein Data Bank, there is a protein that is currently misannotated as an adenine deaminase (entry 2ics). We have purified this protein and have shown that this enzyme is unable to catalyze the deamination of adenine at an appreciable rate.

interest were combined and concentrated to 7.7 mg/mL by centrifugation in an Amicon Ultra-15 10000 molecular weight cutoff centrifugal filter unit. The final yield was 20 mg of protein/L of medium. Electrospray mass spectrometry was used to obtain an accurate mass of the purified protein (64.65 kDa) and confirm complete selenomethionine labeling of 16 methionines. The expression plasmid is available through the PSI: Biology-Materials Repository (<http://psimr.asu.org>) as NYSGXRC clone ID 9206a1BCt6p1, and other experimental information is available in the Protein Expression Purification Crystallization Database (<http://pepcdb.pdb.org>) as TargetID "NYSGXRC-9206a".

Protein and Metal Analysis. The concentration of ADE from *E. coli* was estimated by measuring the absorbance at 280 nm using an extinction coefficient of $42000 \text{ M}^{-1} \text{ cm}^{-1}$ (13). The metal content of the protein was determined by ICP-MS (14). The protein samples for ICP-MS were digested with HNO_3 by refluxing for ~45 min to prevent protein precipitation during the measurement. The protein concentration was adjusted to ~1.0 μM with 1% (v/v) HNO_3 .

Preparation and Reconstitution of the Apo-Enzyme. Apo-ADE was prepared by dialyzing the enzyme purified from the iron-free expression protocol against 10 mM 1,10-phenanthroline in 20 mM HEPES (pH 7.0) for 36 h with two changes of buffer. The apoenzyme was separated from 1,10-phenanthroline using a PD-10 column (GE Healthcare) and then reconstituted with various amounts of Mn^{2+} , Zn^{2+} , or Fe^{2+} at 4 °C for 48 h. In these experiments, 1.0 μM apo-ADE was titrated with the metals mentioned above (0–5 μM). Iron was added anaerobically to prevent air oxidation. All samples were passed through a PD-10 column to remove any unbound metal and then assayed for adenine deaminase activity. The same titration was performed with Atu4426 to establish the metal requirement for this enzyme.

Adenine Deaminase Activity. The deamination of adenine was determined using a coupled assay with glutamate dehydrogenase (GDH). Formation of ammonia was followed at 340 nm using a SpectraMax-340 UV-vis spectrophotometer in the presence of 20 mM HEPES (pH 7.5), 0.15 mM NADH, 25 mM α -ketoglutarate, 4 $\mu\text{g}/\text{mL}$ glutamate dehydrogenase (GDH), and various concentrations of adenine in a final volume of 0.25 or 1.0 mL (15). All the assays were conducted at 30 °C.

Crystallization and Structure Determination of Atu4426. Initial crystallization conditions were identified using the sitting drop vapor diffusion method using the Hampton Research high-throughput screens at 293 K. For screening purposes, 1 μL of protein solution was mixed with 1 μL of precipitant and equilibrated against 130 μL of precipitant. Thin platelike crystals of Atu4426 were obtained with a precipitant solution containing 0.2 M $\text{MgCl}_2 \cdot 6\text{H}_2\text{O}$, 0.1 M HEPES (pH 7.5), and 25% (w/v) PEG 3350. Diffraction quality crystals were obtained using the spot seeding technique performed in 24-well Linbro plates after preequilibration of the crystallization drops (2 μL of protein solution and 2 μL of reservoir solution) against 600 μL of reservoir solution for 24 h.

Crystals were flash-frozen by direct immersion in liquid nitrogen using mother liquor supplemented with 20% (v/v) glycerol. Diffraction data from SeMet crystals were obtained to 2.2 Å resolution using NSLS Beamline X29A (National Synchrotron Light Source, Brookhaven National Laboratory, Upton, NY) and processed with HKL2000 (16). Crystals belong to the monoclinic system, in space group $P2_1$. Crystal parameters and data collection statistics are listed in Table 1.

The crystal structure of Atu4426 was determined by the single-wavelength anomalous dispersion (SAD) with SeMet crystals. Selenium positions in the asymmetric unit were located using SHELXD (17). Heavy atom phase refinement was conducted with SHARP (18), and phases were further improved by density modification (19). Approximately 85% of the polypeptide chain was built automatically with *ARP/wARP* (20). Subsequent model building was performed manually using COOT (21). Rigid-body refinement and restrained refinement were performed using REFMAC (22). Three significant residual densities within the active site in the final $F_o - F_c$ electron density map were modeled as Mn ions. The refined atomic model with an *R* factor of 0.175 was evaluated using the RCSB *AUTODEP* (23) validation tool (<http://www.pdb.org>), and atomic coordinates and structure factor amplitudes were deposited in the Protein Data Bank (PDB) as entry 3nqb. Final refinement statistics for Atu4426 are listed in Table 1.

Model for Binding of Adenine to Atu4426. The ligand-free structure of Atu4426 (chain A) was used for structural modeling. The third metal ion coordinated to His-122, Glu-123, His-477, and Asp-478 was removed. Backbone and side chain conformations of residues near the binuclear metal center (Ser-476–Asn-481 and Asp-120–Gly-125) were explored simultaneously using the "loopmodel" functionality in MODELER-9v2 (24). Thereafter, side chains of residues in these two loops and Met-189, Arg-220, and Asp290 were optimized using the "side chain prediction" protocol in PLOP (25). The refinement of the adenine complex structural model resulted in six good-scoring structural models of Atu4426. The model yielding the greatest enrichment for adenine and the strongest preference of adenine over *N*-6-methyladenine in virtual screening by DOCK against the high-energy intermediate (HEI) database of KEGG molecules was selected to represent the binding mode of adenine in Atu4426 (26–30).

Oxidation and Reduction of the Iron Center. The binuclear metal center of $[\text{Fe}^{\text{II}}/\text{Fe}^{\text{II}}]$ -ADE (100 μM) was oxidized with varying amounts of potassium ferricyanide ranging from 25 to 500 μM at room temperature in 20 mM HEPES (pH 7.5). Aliquots of the enzyme were assayed for catalytic activity after 3 h. $[\text{Fe}^{\text{III}}/\text{Fe}^{\text{III}}]$ -ADE was reduced to $[\text{Fe}^{\text{II}}/\text{Fe}^{\text{II}}]$ -ADE through the anaerobic addition of solid sodium dithionite, and the deaminase activity was determined after incubation for 20, 40, and 60 min. As a control, 2.0 equiv of ferricyanide (40 μM) was added to $[\text{Mn}^{\text{II}}/\text{Mn}^{\text{II}}]$ -ADE (20 μM).

Mössbauer and EPR Spectroscopy. $[\text{Fe}^{\text{II}}/\text{Fe}^{\text{II}}]$ -ADE was prepared for Mössbauer spectroscopy by reconstitution of apo-ADE (300 μM) with 2 equiv of $^{57}\text{FeCl}_3$ (IsoFlex USA) and 2.0 equiv of ascorbic acid at 4 °C for 48 h at pH 7.0 in a volume of 1.2 mL. Samples were passed through a PD-10 column to remove excess metal and then concentrated by ultrafiltration with a YM30 (Millipore) membrane. The spectra were recorded with a MS4 WRC spectrometer (SEE Co., Edina, MN) at either 5 or 100 K and then analyzed using the WMOSS software package provided by the manufacturer. Chemical shifts were calibrated relative to Fe metal at 298 K. EPR spectra were recorded on an EMX X-band spectrometer in perpendicular mode equipped with an Oxford ER910A cryostat (Bruker Biospin, Billerica, MA). Spin concentrations were determined using a 1.0 mM CuEDTA standard. For the $g = 4.3$ signal, double integral values were multiplied by 3 to account for the total spin population of all three doublet levels of the $S = 5/2$ manifold.

Mutation of ADE from *E. coli*. All single-site mutations were constructed using the standard QuikChange PCR protocol

Table 1: Data Collection and Refinement Statistics

cell dimensions	$a = 63.1 \text{ \AA}, b = 131.0 \text{ \AA}, c = 70.00 \text{ \AA}, \beta = 97.8^\circ$
space group	$P2_1$
Data Collection Statistics	
resolution limit (\AA)	39.75–2.2 (2.28–2.2) ^d
no. of unique reflections	56338 (5593) ^d
completeness (%)	99.9 (99.9) ^d
R_{merge}^a (%)	0.119 (0.463) ^d
$\langle I/\sigma(I) \rangle$	9.8 (2.0) ^d
no. of molecules per asymmetric unit	2
Phasing Statistics	
phasing power ^b (ano)	1.47
figure of merit ^c (centric/acentric)	0.056/0.348
figure of merit after density modification	0.93
Refinement Statistics	
no. of protein atoms	8672
no. of ligand atoms	6
no. of solvent atoms	380
R_{cryst} (%)	17.5
R_{free} (%)	23.5
mean B factor (\AA^2)	26.23
Root-Mean-Square Deviations	
bond lengths (\AA)	0.021
bond angles (deg)	1.904
Ramachandran Plot Statistics (%)	
residues in allowed regions	89.2
residues in additionally allowed regions	9.5

^a $R_{\text{merge}} = \sum |I_i - \langle I \rangle| / \sum I_i$, where I_i is the intensity of the i th measurement and $\langle I \rangle$ the mean intensity for that reflection. ^bPhasing power as defined in SHARP. ^cFigure of merit as defined in SHARP. ^dValues for the highest-resolution shell are given in parentheses.

according to the manufacturer's instructions. All of the mutants were expressed and purified using the iron-free expression protocol. The apoproteins (20 μM) were purified as described earlier and reconstituted with 2.0 enzyme equivalents of Fe^{2+} (40 μM) under anaerobic conditions. Excess metal was removed using a PD-10 column, and the metal content was measured using ICP-MS. In an attempt to rescue the loss of activity of the E185G mutant, various concentrations of propionic acid (0.5–10 mM) and Mn^{2+} (0.1–1.0 mM) were added to the apo-E185G mutant and allowed to incubate for 6 h in 200 mM HEPES (pH 7.5) at 4 °C.

pH–Rate Profiles. The dependence of k_{cat} and k_{cat}/K_m as a function of pH was determined for the Mn^{2+} , Zn^{2+} , and Fe^{2+} -reconstituted ADE over the pH range of 6.0–9.0. The following buffers were used: 20 mM MES (pH 6.0–6.6), 20 mM HEPES (pH 6.8–8.2), and 20 mM CHES (pH 8.4–9.0). The pH values of the final solutions were measured before and after the completion of the assays. Above pH 9, the coupling system was inefficient, and below pH 6, ADE was unstable. Equivalent profiles were also obtained in 100% D_2O .

Solvent Viscosity Effects. The effects of solvent viscosity on k_{cat} and k_{cat}/K_m of [Mn/Mn]-ADE were determined at pH 7.5 with 50 mM HEPES at 30 °C. The viscosity was varied by increasing the concentration of sucrose (31).

Inhibition of ADE by 6-Chloropurine. The inhibition of ADE by 6-chloropurine was evaluated by incubation of [Mn/Mn]-ADE (4 nM) with varying concentrations of 6-chloropurine at 30 °C for 1 h. Aliquots were removed and assayed for the deamination of 5.0 mM adenine at pH 7.5 and 30 °C.

Data Analysis. Initial velocity data were fit to eq 1 using the nonlinear least-squares fitting program SigmaPlot 9.0

$$v/E_t = k_{\text{cat}}[A]/(K_m + [A]) \quad (1)$$

where v is the initial velocity, $[A]$ is the substrate concentration, E_t is the total enzyme concentration, k_{cat} is the turnover number, and K_m is the Michaelis constant. For pH–rate profiles, eq 2 was used to fit the bell-shaped pH profiles to determine values of K_a and K_b , for the ionization of groups at low and high pH values, respectively.

$$\log y = \log[c/(1 + [H]/K_a + K_b/[H])] \quad (2)$$

where c is the maximal value for either k_{cat} or k_{cat}/K_m , depending on the fit, and $[H]$ is the proton concentration. The tight binding inhibition constant for binding of 6-chloropurine to ADE was obtained using eq 3 (32).

$$v_i/v_o = \{E_t - K_i - [I] + [(I) + K_i - E_t]^2 + 4K_i E_t\}^{1/2} / (2E_t) \quad (3)$$

where E_t is the total enzyme concentration, $[I]$ is the inhibitor concentration, v_o is the activity of the enzyme in the absence of inhibitor, and v_i is the activity of the enzyme in the presence of varying inhibitor concentrations.

RESULTS

Purification and Properties of ADE. Adenine deaminase from *E. coli* was purified to apparent homogeneity. The enzyme purified in the presence and absence of added Mn^{2+} displayed

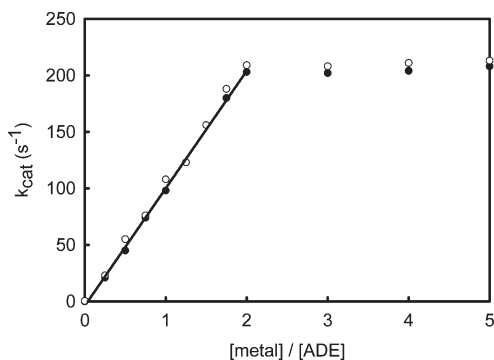


FIGURE 1: Titration of varying enzyme equivalents of Mn^{2+} (O) and Fe^{2+} (●) to apo-ADE from *E. coli* (1.0 μM) at 4 °C. The enzyme assays were performed after the mixture of apo-ADE and metal had been allowed to equilibrate for 48 h at pH 7.5. The reconstitution with iron was conducted anaerobically. Similar experiments were conducted with Zn^{2+} (data not shown).

similar kinetic properties and heterogeneous metal content. The kinetic constants for the enzyme purified without Mn^{2+} supplementation were $1.6 \pm 0.2 \text{ s}^{-1}$, $0.81 \pm 0.08 \text{ mM}$, and $(2.0 \pm 0.2) \times 10^3 \text{ M}^{-1} \text{ s}^{-1}$ (k_{cat} , K_{m} , and $k_{\text{cat}}/K_{\text{m}}$, respectively). This enzyme contained 0.25 ± 0.05 equiv of Fe and 0.20 ± 0.03 equiv of Zn per subunit. The kinetic constants for the enzyme purified with Mn^{2+} supplementation in the growth medium were $2.0 \pm 0.3 \text{ s}^{-1}$, $0.76 \pm 0.1 \text{ mM}$, and $(2.5 \pm 0.2) \times 10^3 \text{ M}^{-1} \text{ s}^{-1}$ (k_{cat} , K_{m} , and $k_{\text{cat}}/K_{\text{m}}$, respectively). This sample contained 0.31 ± 0.04 equiv of Fe and 0.24 ± 0.03 equiv of Mn per subunit. The kinetic constants for Atu4426 purified using the standard expression protocol were $1.8 \pm 0.2 \text{ s}^{-1}$, $0.40 \pm 0.08 \text{ mM}$, and $(4.5 \pm 0.4) \times 10^3 \text{ M}^{-1} \text{ s}^{-1}$ (k_{cat} , K_{m} , and $k_{\text{cat}}/K_{\text{m}}$, respectively). Atu4426 purified using standard protocols contained 0.80 ± 0.05 equiv of Fe and 0.41 ± 0.05 equiv of Mn per subunit.

Sequestration of Iron. The addition of 50 μM 2,2'-dipyridyl to the growth medium was utilized to sequester the iron at the time of induction. The cells were supplemented with Mn, and the purified enzyme contained 2.0 ± 0.1 equiv of Mn per protein subunit. The kinetic constants for the deamination of adenine by *E. coli* ADE were determined to be $200 \pm 5 \text{ s}^{-1}$, $0.40 \pm 0.04 \text{ mM}$, and $(5 \pm 0.4) \times 10^5 \text{ M}^{-1} \text{ s}^{-1}$ (k_{cat} , K_{m} , and $k_{\text{cat}}/K_{\text{m}}$, respectively).³ The kinetic constants for the deamination of adenine by Atu4426 were determined to be $155 \pm 5 \text{ s}^{-1}$, $0.32 \pm 0.04 \text{ mM}$, and $(4.8 \pm 0.4) \times 10^5 \text{ M}^{-1} \text{ s}^{-1}$ (k_{cat} , K_{m} , and $k_{\text{cat}}/K_{\text{m}}$, respectively). The iron-free expression protocol yielded a protein with 2.4 ± 0.1 equiv of Mn per protein subunit for Atu4426. All of the remaining experiments were conducted with protein expressed in *E. coli* from cells grown in the presence of the iron chelator.

Reconstitution of the Apoenzyme. Apo-ADE from *E. coli* was prepared by dialysis of [Mn/Mn]-ADE with 10 mM 1,10-phenanthroline at pH 7.0. The apoenzyme had less than 0.2% of the original adenine deaminase activity, and removal of manganese was confirmed by ICP-MS. Apo-ADE was reconstituted with variable amounts of Mn^{2+} , Zn^{2+} , or Fe^{2+} for 48 h at pH 7.5 and 4 °C to determine the stoichiometry of metal ion and protein

Table 2: Kinetic Parameters and Metal Content of Metal-Reconstituted Forms of *E. coli* ADE^a

enzyme	K_{m} (mM)	k_{cat} (s^{-1})	$k_{\text{cat}}/K_{\text{m}}$ ($\text{M}^{-1} \text{ s}^{-1}$)	no. of metals per subunit
[Mn/Mn]-ADE	0.30 ± 0.03	185 ± 5	$(6.1 \pm 0.5) \times 10^5$	2.0 ± 0.1
[Zn/Zn]-ADE	0.23 ± 0.02	123 ± 8	$(5.4 \pm 0.5) \times 10^5$	1.9 ± 0.1
[Fe/Fe]-ADE	0.33 ± 0.03	196 ± 3	$(5.9 \pm 0.5) \times 10^5$	1.9 ± 0.1

^apH 7.5 and 30 °C.



FIGURE 2: Ribbon representation of the structure of Atu4426. The polypeptide segments consisting of residues 9–87 and 338–375 of the N-terminal domain are colored purple and cyan, respectively. TIM barrel and C-terminal domains are colored green and marine blue, respectively. Loop residues 376–386, connecting the N- and C-terminal domains, are colored brown. The manganese ions are shown as magenta spheres.

required for optimal catalytic activity. There was a linear increase in catalytic activity as the concentration of the divalent cation was increased from 0 to 2 equiv relative to the subunit concentration. The titrations are shown in Figure 1. These titrations confirm that two metal ions are required for the optimal catalytic activity of ADE, and the linearity of the titration curve is consistent with a cooperative assembly of the binuclear metal center (33). The kinetic constants and metal content of the reconstituted forms of ADE from *E. coli* are listed in Table 2. The Mn^{2+} -reconstituted ADE has essentially the same turnover number (196 s^{-1}) as the enzyme isolated from *E. coli* (200 s^{-1}). The elution of adenine deaminase from the gel filtration column supports an oligomeric structure as a homodimer (data not shown). Apo-Atu4426 was prepared by dialysis, and the absence of metal was confirmed by ICP-MS. The reconstitution of Atu4426 with Mn^{2+} and Fe^{2+} (anaerobically) resulted in metal activation profiles identical to those obtained for the *E. coli* ADE shown in Figure 1 (see Figure S1 of the Supporting Information).

Three-Dimensional Structure of Atu4426. The asymmetric unit contains two protomers that are very similar to one another (rmsd of 0.26 Å). Each protomer contains three domains: an N-terminal β -sandwich, a TIM barrel, and a C-terminal α/β -domain shown in Figure 2. Polypeptide segments consisting of residues 9–87 and 338–375 form the N-terminal β -sandwich domain with two terminal α -helices. The C-terminal α/β -domain (residues 387–595) consists of an eight-stranded twisted β -sheet with α -helices flanking it on either side. A classical TIM barrel domain (residues 88–337) bridges these two domains and forms the core of the structure. A long loop (residues 376–386) connects the N- and C-terminal domains and passes on the side of the TIM barrel domain. Metal binding sites are located in the cavity at the interface formed by the amino acids from the TIM barrel and C-terminal domains. The binuclear manganese center

³Mass spectrometry of adenine deaminase that was expressed and purified from *E. coli* without the use of a chelator to suppress the concentration of iron at the time of induction established that the protein was oxygenated at multiple histidine and methionine residues that were at or near the active site. These modifications to the active site explain the differences in the values of k_{cat} between the enzyme preparations obtained from cells grown in the presence or absence of the iron chelator. These experiments will be reported at a later date.

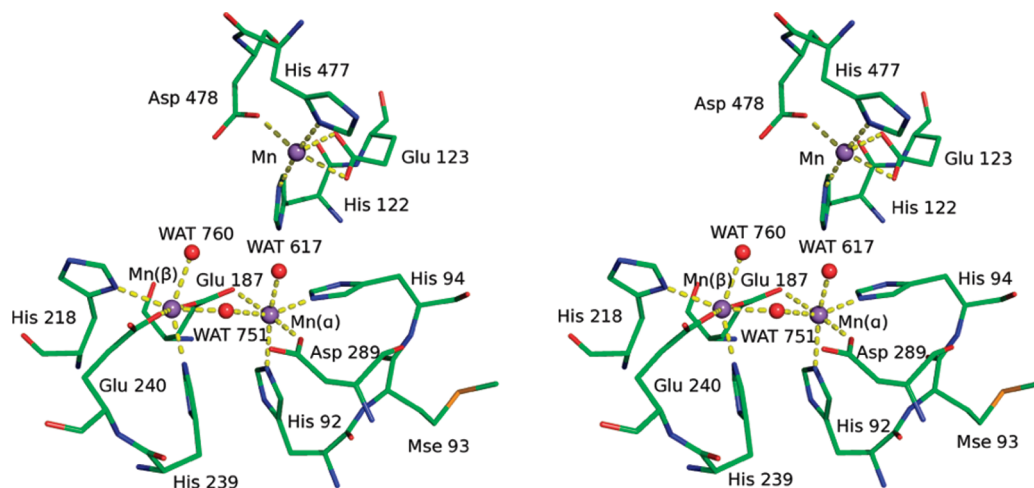


FIGURE 3: Stereoview of the Atu4426 active site residues. Metal ions and coordinating water molecules are colored gray and red, respectively.

is formed from amino acid residues of the TIM barrel domain, whereas the secondary manganese site is formed from residues of the TIM barrel and C-terminal domain and bridges the two domains.

The active site of Atu4426 contains three Mn^{2+} ions (Figure 3). A stereoview of the active site is presented in Figure 3. The first two metal ions form a binuclear metal center that is similar, but not identical, to those of other members of the amidohydrolyase superfamily (4, 5). The HxH motif (His-92 and His-94) from β -strand 1 and the aspartate (Asp-289) from β -strand 8 coordinate the α -metal ion. The β -metal ion is ligated by His-218 from β -strand 5 and His-239 and Glu-240 (both from β -strand 6). The two metal ions are bridged to one another by Glu-187 (from β -strand 4) and a hydroxide/water from solvent. A model of the active site is presented in Figure 4A. The third metal ion is coordinated to His-122, Glu-123, His-477, and Asp-478 and is 6.6 Å from the α -metal and 8.2 Å from the β -metal of the binuclear metal center.

Model of Adenine Bound in the Active Site. A comparison between the binding site in the ligand-free crystal structure and the binding site in the proposed model is presented in Figure 4A. The model of the binuclear metal center (His-92, His-94, Glu-187, His-218, His-239, and Asp-289) is nearly identical to that in the crystal structure. The differences include the side chain of Arg-220 that is rotated by $\sim 90^\circ$ so that the guanidino group is not in the proximity of the binuclear metal center. Model side chains of Glu-240 and Asp-290 were adjusted to result in more favorable electrostatic interactions between the carboxylate groups and the two metals. Furthermore, His-122, Glu-123, and His-477 form a more closed ligand-binding site in comparison to the open conformation in the crystal structure. The best-scored binding pose of adenine in the modeled binding site is shown in Figure 4B. The tetrahedral intermediate was formed by the bridging hydroxide attacking C-6 on the *re* face of adenine. In this complex, the ammonia leaving group forms hydrogen bonds with the side chains of Asp-289 and Asp-290. The protonated N-1 atom of adenine forms hydrogen bonds with the side chain of Glu-240. In addition, the N-7 atom of adenine coordinates the α -metal, and the N-9 (NH) atom forms hydrogen bonds with the side chain of Glu-123. The N ϵ atom in His-122, which was assigned to be protonated during modeling, is adjacent to the N-3 atom of adenine (3.7 Å) and OE2 of Glu-123 (3.1 Å).

Substrate Specificity. A number of compounds having adenine-like moieties were tested as substrates or competitive

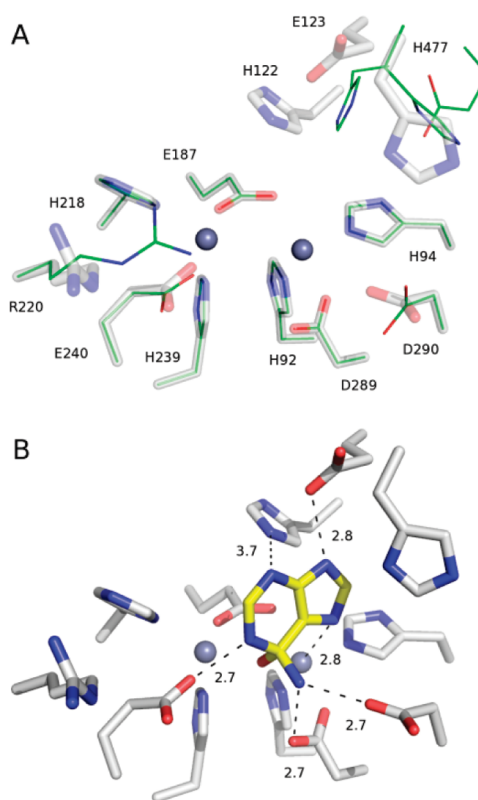


FIGURE 4: (A) Binding site conformation in the model of Atu4426 (transparent sticks) compared to the binding site in the ligand-free crystal structure of Atu4426 (solid line). The two metal ions in the model are colored dark blue, occupying places identical to those of the two metal ions in the crystal structure. (B) Binding mode of the tetrahedral intermediate formed during the deamination of adenine in the modeled binding site of Atu4426, predicted by docking with DOCK. Polar contacts between adenine and binding site residues are denoted with dashed lines with distances given in angstroms.

inhibitors for ADE from *E. coli*. Among these compounds were 2-hydroxyadenine, *N*-6-methyladenine, 6-chloropurine, 7-methyladenine, 2,6-diaminopurine, adenosine, 6-methoxypurine, 6-methylpurine, 6-mercaptopyrimidine, and 6-methylmercaptopyrimidine. 6-Chloropurine was a very effective tight binding inhibitor for ADE from *E. coli*. However, none of the other compounds was either a substrate or competitive inhibitor for ADE.

EPR and Mössbauer Spectroscopy of [Fe/Fe]-ADE. The 5 K low-field Mössbauer spectrum of the reconstituted and fully

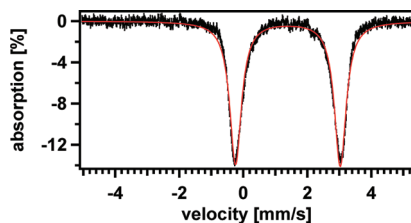


FIGURE 5: Mössbauer spectrum of $[\text{Fe}^{\text{II}}/\text{Fe}^{\text{II}}]$ -ADE ($265 \mu\text{M}$). The spectrum was recorded at 5 K with a 400 G magnetic field applied parallel to the radiation. The red line represents a simulation for which $\delta = 1.39 \text{ mm/s}$ and $\Delta E_{\text{q}} = 3.27 \text{ mm/s}$ with a line width of 0.47 mm/s .

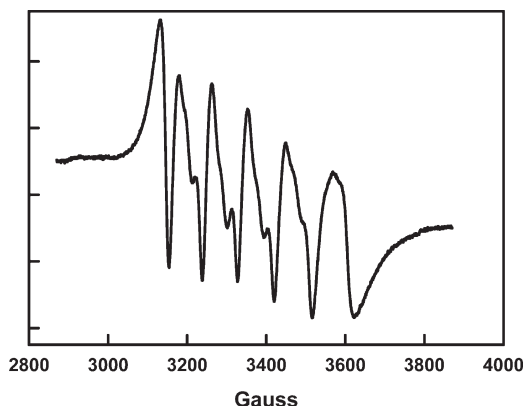


FIGURE 6: EPR spectrum of $220 \mu\text{M}$ $[\text{Mn}/\text{Mn}]$ -ADE recorded at 10 K with a 9.46 GHz microwave power of 0.02 mW.

active $[\text{Fe}/\text{Fe}]$ -ADE (Figure 5) exhibited a quadrupole doublet typical of high-spin Fe^{II} ions (34). Line shapes and line widths revealed no evidence of multiple species. Given the presence of two irons per protein, this suggests a very similar ligand environment for both ferrous ions. The enzyme in the $[\text{Fe}^{\text{II}}/\text{Fe}^{\text{II}}]$ state was EPR-silent. To determine whether $[\text{Fe}^{\text{II}}/\text{Fe}^{\text{II}}]$ -ADE is air-sensitive, this protein was incubated aerobically at room temperature and then assayed for catalytic activity. There was no loss of activity after 24 h, and the Mössbauer spectrum (not shown) demonstrated that the iron remained high-spin ferrous. The EPR spectrum of $[\text{Mn}/\text{Mn}]$ -ADE showed a prototypical six-line pattern for Mn^{2+} (Figure 6) with no evidence of antiferromagnetic coupling (35). The use of a higher microwave power and an elevated temperature for the EPR spectra did not provide any evidence of coupling between the two Mn ions within the binuclear metal center (data not shown).

Oxidation and Reduction of $[\text{Fe}/\text{Fe}]$ -ADE. Potassium ferricyanide was used to oxidize the binuclear metal center to determine if the diferric state of the binuclear metal center is active for the deaminase reaction. Increasing ferricyanide to $[\text{Fe}^{\text{II}}/\text{Fe}^{\text{II}}]$ -ADE ($100 \mu\text{M}$) concentration ratios linearly inactivated the catalytic activity (Figure 7) with 2 equiv of the reagent being sufficient to fully inactivate the enzyme. The Mössbauer spectrum of iron-bound ADE treated with 2 equiv of ferricyanide exhibited a six-line pattern typical of a high-spin ferric oxidation state (Figure 8A). The EPR spectrum of $[\text{Fe}^{\text{III}}/\text{Fe}^{\text{III}}]$ -ADE exhibited a $g = 4.3$ signal, typical of Fe^{III} ions with rhombic symmetry (Figure 8B). The spin concentration of the signal corresponded to 1.9 spins/mol of protein, suggesting that the ferric ions are not magnetically interacting and that each ion affords the EPR signal. $[\text{Fe}^{\text{III}}/\text{Fe}^{\text{III}}]$ -ADE was reduced back to the diferrous state with the anaerobic addition of sodium dithionite, and the deaminase activity

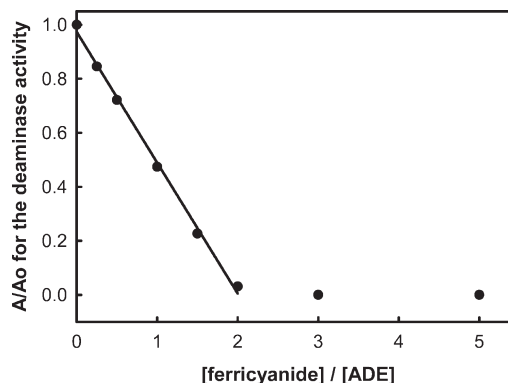


FIGURE 7: Loss of adenine deaminase activity after the addition of various amounts of potassium ferricyanide to $100 \mu\text{M}$ $[\text{Fe}^{\text{II}}/\text{Fe}^{\text{II}}]$ -ADE.

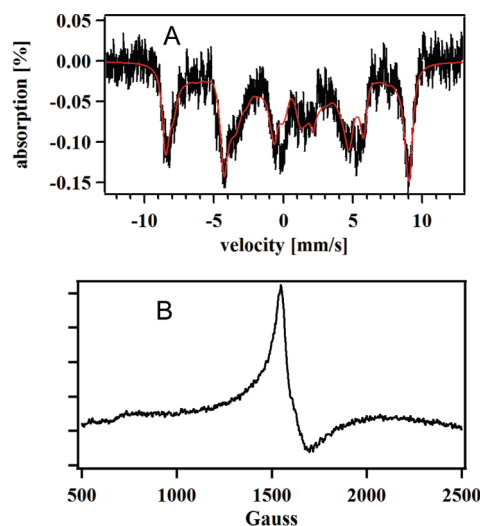


FIGURE 8: (A) Mössbauer spectrum of $[\text{Fe}/\text{Fe}]$ -ADE ($200 \mu\text{M}$) after the addition of 2 equiv of ferricyanide ($400 \mu\text{M}$). Collection parameters: temperature, 5 K; field, 700 G; counts of radiation, 2.2×10^7 . The red line is a simulation assuming a single species with the following parameters: $D = 0.129$, $E/D = 0.194$, $g_x = g_y = g_z = 2.0$, $\Delta E_{\text{q}} = 0 \text{ mm/s}$, $\eta = -1.00$, $A_x = A_y = A_z = -222 \text{ kG}$, $\delta = 0.50 \text{ mm/s}$, and $\Gamma = 0.50 \text{ mm/s}$. (B) EPR spectrum of $200 \mu\text{M}$ $[\text{Fe}^{\text{III}}/\text{Fe}^{\text{III}}]$ -ADE after treatment with ferricyanide. EPR parameters: temperature, 10 K; microwave power, 0.2 mW; microwave frequency, 9.46 GHz.

was fully reconstituted within 1 h. The Mössbauer spectrum of this sample (data not shown) resembled the spectrum of $[\text{Fe}^{\text{II}}/\text{Fe}^{\text{II}}]$ -ADE shown in Figure 5. Addition of 0.25 mM H_2O_2 to $1.5 \mu\text{M}$ $[\text{Fe}^{\text{II}}/\text{Fe}^{\text{II}}]$ -ADE resulted in the irreversible oxidation of the iron center and oxygenation of the protein.

Mutagenesis of ADE. Amino acid sequence alignments and the X-ray structure of Atu4426 indicate that His-90, His-92, Glu-185, His-214, His-235, Glu-236, and Asp-284 are the direct metal ligands to the binuclear metal center of ADE from *E. coli*. Mutation of His-92, His-214, His-235, and Glu-185 resulted in the total loss of catalytic activity as well as the ability to bind divalent metals in the active site. The D284A and E236Q mutants were able to bind 2 equiv of Mn^{2+} or Fe^{2+} in the active site, but these mutants were unable to catalyze the deaminase reaction. The H90N mutant was able to bind ~ 2 equiv of Mn^{2+} or Fe^{2+} per monomer and had a k_{cat} of $\sim 5\%$ of the wild-type enzyme. The H90C and H90D mutants were unable to bind either iron or manganese.

Table 3: Catalytic Constants and Metal Binding Properties of *E. coli* ADE Mutants

mutant	K_m (mM)	k_{cat} (s^{-1})	k_{cat}/K_m ($M^{-1} s^{-1}$)	Mn/subunit
H90D	0.44 ± 0.04	0.036 ± 0.004	82 ± 8	0.022 ± 0.004
H90C	0.51 ± 0.05	0.053 ± 0.008	103 ± 9	0.032 ± 0.003
H90Q	0.40 ± 0.03	0.8 ± 0.1	$(2.0 \pm 0.2) \times 10^3$	0.043 ± 0.002
H90N	0.35 ± 0.03	8.0 ± 1.2	$(2.2 \pm 0.3) \times 10^4$	1.8 ± 0.2
H92D	0.38 ± 0.04	0.8 ± 0.1	$(2.1 \pm 0.3) \times 10^3$	0.12 ± 0.05
H92C	0.45 ± 0.04	0.69 ± 0.08	$(1.4 \pm 0.2) \times 10^3$	0.23 ± 0.05
H92Q	0.48 ± 0.05	0.08 ± 0.03	166 ± 12	0.08 ± 0.01
H92N	0.42 ± 0.03	0.05 ± 0.01	119 ± 10	0.13 ± 0.03
S95A	0.47 ± 0.04	78 ± 2	$(1.6 \pm 0.2) \times 10^5$	2.1 ± 0.1
D118N	0.35 ± 0.03	173 ± 2	$(5.6 \pm 0.3) \times 10^5$	2.1 ± 0.1
H120N	0.47 ± 0.05	0.13 ± 0.01	361 ± 17	2.1 ± 0.1
E121Q	0.44 ± 0.04	57 ± 1	$(1.3 \pm 0.2) \times 10^5$	2.0 ± 0.1
E185Q	1.6 ± 0.4	0.06 ± 0.005	38 ± 4	0.030 ± 0.001
E185G	not determined	$< 5 \times 10^{-4}$	not determined	0.008 ± 0.001
H214Q	0.32 ± 0.03	1.3 ± 0.2	$(4.0 \pm 0.5) \times 10^3$	0.33 ± 0.05
H214N	0.37 ± 0.4	0.5 ± 0.2	$(1.3 \pm 0.3) \times 10^3$	0.12 ± 0.06
H235D	0.48 ± 0.05	1.2 ± 0.08	$(2.5 \pm 0.3) \times 10^3$	0.42 ± 0.05
H235C	1.2 ± 0.2	1.5 ± 0.1	$(1.3 \pm 0.2) \times 10^3$	0.34 ± 0.05
H235Q	0.80 ± 0.11	1.3 ± 0.1	$(1.6 \pm 0.3) \times 10^3$	0.23 ± 0.05
H235N	0.82 ± 0.09	0.5 ± 0.1	609 ± 35	0.33 ± 0.05
E236Q	0.41 ± 0.04	0.072 ± 0.002	170 ± 16	1.8 ± 0.1
D284A	0.86 ± 0.07	0.022 ± 0.005	26 ± 5	1.9 ± 0.2
D285A	0.32 ± 0.04	37 ± 2	$(1.3 \pm 0.2) \times 10^5$	2.1 ± 0.1
H473N	0.32 ± 0.03	178 ± 2	$(5.6 \pm 0.3) \times 10^5$	2.0 ± 0.1
D474N	0.31 ± 0.03	171 ± 2	$(5.5 \pm 0.2) \times 10^5$	1.9 ± 0.2

The S95A, D118N, H120N, E121Q, E236Q, D285A, H473N, and D474N mutants were constructed on the basis of the conservation of residues in the active site and the working model of adenine bound in the active site of Atu4426 (Figure 4). All of these mutants are able to bind approximately two metals per active site. The kinetic constants and metal content for the mutants are listed in Table 3. The reconstitution of apo-E185G with propionic acid and Mn^{2+} was conducted to establish the role of the carboxylate side chain of Glu-185 as a bridge for the binuclear metal center. The addition of 10 mM propionic acid and 1.0 mM Mn^{2+} to 5.0 nM apo-E185G resulted in the reconstitution of $\sim 85\%$ of the activity of the wild-type enzyme ($k_{cat} \sim 168 s^{-1}$).

pH-Rate Profiles. The kinetic constants for the deamination of adenine by ADE were obtained as a function of pH, and the profiles are shown in Figure 9. The pH profiles for k_{cat} and k_{cat}/K_m are bell-shaped. Similar results were obtained for the profiles in D_2O , the exception being that the values of k_{cat} and k_{cat}/K_m are doubled in D_2O with an inverse solvent isotope effect of 0.49 ± 0.02 at pH 7.5. The pK_a values are listed in Table 4.

Solvent Viscosity Effects. Increasing solvent viscosity had a small effect on the relative values of k_{cat} and k_{cat}/K_m for the deamination of adenine. At pH 7.5, the slope for the k_{cat} profile was 0.020 ± 0.002 and the slope for the k_{cat}/K_m profile was 0.18 ± 0.02 (data not shown).

Inhibition by 6-Chloropurine. ADE was incubated with various concentrations of 6-chloropurine for 1 h and then assayed for catalytic activity. The deaminase activity decreased with an increase in the concentration of 6-chloropurine when the adenine concentration was fixed at 5.0 mM. The K_i for 6-chloropurine was determined to be 130 ± 15 nM from a fit of the data to eq 3.

DISCUSSION

Metal Requirement. Fully active ADE was successfully purified from *E. coli* only when the iron in the growth medium

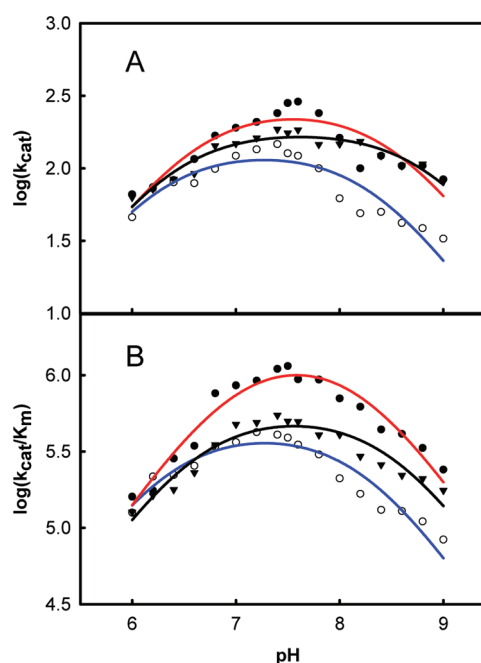


FIGURE 9: pH-rate profiles for the different metal-reconstituted forms of ADE. The line for [Fe/Fe]-ADE (●) is colored red, the line for [Zn/Zn]-ADE (○) blue, and the line for [Mn/Mn]-ADE (▼) black. The lines represent fits of the data to eq 2.

was sequestered with a suitable chelator. The isolated enzyme under these conditions contained two manganese ions in the active site. The turnover number for the deamination of adenine ($\sim 200 s^{-1}$) is approximately 2 orders of magnitude greater than that for any ADE previously reported in the literature (1, 2). [Mn/Mn]-ADE is stable, and apo-ADE can be prepared from this enzyme form by chelation of the metal ions with *o*-phenanthroline. Apo-ADE can be reconstituted with 2 equiv of Zn^{2+} , Fe^{2+} , or Mn^{2+} . The linear increase in the catalytic activity when

Table 4: Kinetic pK_a Values Obtained for ADE in H_2O and D_2O

metal reconstitution	k_{cat}		k_{cat}/K_m	
	pK_a	pK_b	pK_a	pK_b
H_2O				
Fe/Fe	6.6 ± 0.1	8.5 ± 0.1	6.3 ± 0.1	8.2 ± 0.1
Zn/Zn	6.4 ± 0.1	8.6 ± 0.1	6.6 ± 0.1	8.5 ± 0.1
Mn/Mn	6.2 ± 0.2	8.3 ± 0.1	6.9 ± 0.1	8.2 ± 0.1
D_2O				
Fe/Fe	6.1 ± 0.1	8.7 ± 0.1	6.5 ± 0.1	8.3 ± 0.1
Zn/Zn	6.7 ± 0.1	8.4 ± 0.1	6.9 ± 0.1	8.1 ± 0.1
Mn/Mn	6.5 ± 0.1	8.6 ± 0.1	6.5 ± 0.1	8.3 ± 0.1

0–2 equiv of these cations is added to apo-ADE is consistent with the cooperative formation of a binuclear metal center (33). $[Fe^{II}/Fe^{II}]$ -ADE prepared in this manner is as active for the deamination of adenine as $[Mn/Mn]$ -ADE and $[Zn/Zn]$ -ADE, and this enzyme also remains catalytically active in the presence of oxygen overnight at room temperature. Similar results were observed for the reconstitution of apo-Atu4426 with metal, indicating that the binuclear metal center is critical for the deaminase activity of Atu4426.

Seven amino acid residues in the active site that bind to either of the two divalent cations were changed and the mutant proteins characterized. Metal binding and catalytic activity were lost upon the single-site mutation of His-92, Glu-185, His-214, or His-235. Metal binding was also disrupted when His-90 was mutated to aspartate, cysteine, or glutamine, but not asparagine. Mutation of Asp-284 and Glu-236 to alanine and glutamine, respectively, did not disrupt the binding of metal to the active site. However, the D284A and E236Q mutants were inactive as an adenine deaminase. These results are consistent with the formation of a binuclear metal center in which one metal ion is coordinated to His-90 and His-92 while the second metal ion is coordinated to His-214 and His-235. This model is confirmed by the three-dimensional structure determination of Atu4426. The two metal ions are bridged by Glu-185 and a bridging water/hydroxide. The conserved aspartate residue from β -strand 8 and the glutamate from β -strand 6 are not essential for metal binding, but they are critical for the activation of water and protonation of the transition state to form the reaction products.

Oxidative State of Iron. Mössbauer spectroscopy (in conjunction with the absence of an EPR signal) demonstrates that both Fe ions in reconstituted and catalytically active $[Fe/Fe]$ -ADE are high-spin ferrous. A single quadrupole doublet was observed, and the inability of Mössbauer spectroscopy to distinguish between the two irons suggests that the environment of both irons is similar. The presence of a $g = 4.3$ EPR signal in the ferricyanide-oxidized state, along with the metal analysis showing two irons per ADE and low-field Mössbauer spectra showing a six-line pattern, indicates that the ferric ions are high-spin $S = 5/2$ and magnetically isolated rather than being magnetically coupled. Our data provide no evidence of whether the two ferrous ions are spin-coupled. However, given the general lack of coupling in the diferric state, we suspect that the two ferrous ions are not spin-coupled. $[Fe^{II}/Fe^{II}]$ -ADE can be oxidized to $[Fe^{III}/Fe^{III}]$ -ADE by the addition of ferricyanide, but this enzyme is unable to catalyze the deamination of adenine. The $[Fe^{III}/Fe^{III}]$ -ADE can, however, be reduced back to $[Fe^{II}/Fe^{II}]$ -ADE by the addition of dithionite with full recovery of catalytic activity.

Therefore, oxidation of the metal center with ferricyanide does not irreversibly damage the active site. These experiments demonstrate that the active deaminase is in the diferrous state and that the two metals are not easily oxidized by air to the diferric state.

Addition of H_2O_2 results in the irreversible oxidation of diferrous ADE to diferric ADE and protein damage. However, the addition of hydrogen peroxide to $[Mn/Mn]$ -ADE has no effect. Enzyme treated with H_2O_2 can be reduced to the diferrous form, but no deaminase activity could be reconstituted. These results suggest that irreversible oxygenation reactions are occurring after the addition of H_2O_2 to $[Fe^{II}/Fe^{II}]$ -ADE, possibly because of the generation of hydroxyl radicals (36).

pH-Rate Profiles. The pH-rate profiles are bell-shaped. This result is consistent with two groups being involved in catalysis, one of which is protonated and the other unprotonated for optimal activity. The pH-rate profiles also indicate a fairly broad pH range over which the deaminase activity occurs. The optimal pH is ~ 7.5 . The various metal-reconstituted forms of ADE do not significantly change the kinetic pK_a values of the groups involved in catalysis. The structure of adenine deaminase from *A. tumefaciens* can be used to assist in the identification of residues involved in catalysis. On the basis of previous studies for other members of the AHS, it is likely that the pK_a of ~ 6.4 reflects the ionization of Asp-284, the highly conserved residue at the end of β -strand 8, or the protonation of the bridging hydroxide. Asp-284 must be unprotonated and is critical for the activation of the hydrolytic water molecule. Mutation of this residue (D284A) confirms that this residue is essential for the deamination of adenine. The second ionization with a kinetic pK_a of ~ 8.5 is assigned for the highly conserved glutamate residue from β -strand 6 that coordinates one of the metal ions. The E236Q mutant retains the metal binding properties of ADE, but this mutant is inactive to the deaminase activity. This result is consistent with this residue protonating N-1 of the purine ring during the formation of hypoxanthine.

Solvent Isotope Effects. The reaction catalyzed by ADE in D_2O is twice as fast as that in H_2O , giving an inverse isotope effect of ~ 0.5 for both k_{cat} and k_{cat}/K_m . Large inverse isotope effects have been seen for other members of the AHS superfamily catalyzing different deaminase reactions. For example, adenosine deaminase (37, 38) and adenosine monophosphate deaminase (39) have inverse solvent isotope effects of 0.45 ± 0.04 and 0.71 ± 0.07 , respectively (37, 39). In all cases, the large inverse isotope effect has been attributed to a compressed hydrogen bond in the transition state, where the pK_a values of the acceptor and donor groups are fairly close or similar (37, 38). For ADE from *E. coli*, this means that the protonated form of Glu-236 and the N-1 atom of the purine moiety of adenine have a fairly close pK_a , which allows the protonation of N-1, concomitant with hydrolytic attack at C-6. Analogous to the model described by Cleland (38) for adenosine deaminase, once the OH group adds to C-6 of the adenine moiety, the pK_a of N-1 increases relative to that of the protonated form of Glu-236. This increase would allow the transfer of a proton from Glu-236 to the N-1 atom of adenine.

Proposed Mechanism of Action. ADE requires two divalent cations for catalytic activity. The X-ray structure of Atu4426 also shows a third metal in the active site, coordinated to His-120, Glu-121, His-473, and Asp-474. These residues were mutated to assess the effects on metal binding capacity and catalytic activity. The metal binding capacity of these mutants was found to be ~ 2.0 per monomer of ADE. These results suggest that the

Scheme 2

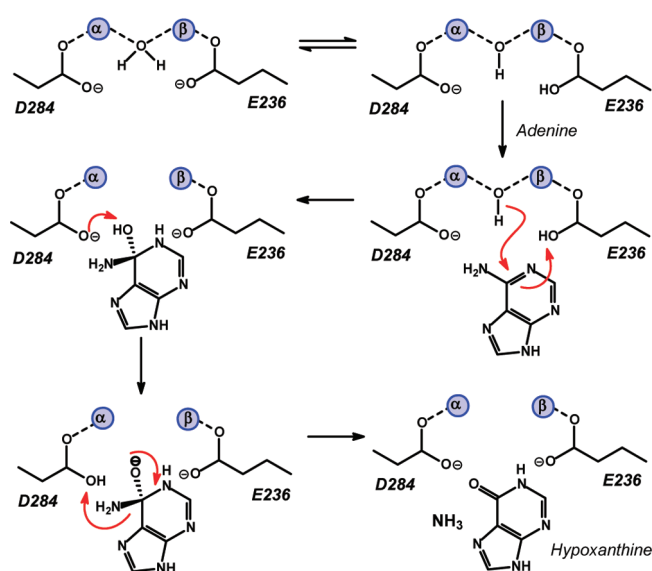
<i>E. coli</i> Atu4426	GDAVADYIIDNVSI LD LINGGEISGPIV IK GRYIAGVGA YTD APALQRIDARGATAVPG 85 GDQRF DV LITGGT LV DVV TG ELRPADIGIVGALIASVHEPASRRDAAQVIDAGGAYVSPG 87
<i>E. coli</i> Atu4426	FIDAH LL HIE S SMMPVT F ETATL PR GLTT V ICDP HE IVNVMGEAGFAWFARCAEQARQ NQ 145 LIDT HM HIE S SMITPAAYAAAVVARGV TT IVWDP HE FGNVHGV DG V R WAAKAIENLPLRA 147
<i>E. coli</i> Atu4426	YLQVSSCVPALEGC D VNGASF---TLEQMLAWRDHPQVTGLA E MMDPG V ISGQ N ALLDK 202 ILLAPSCVPSAPGLERGGADF DA AILADLLSW---PEIGGIA E IMNMRGVI ER DPRMSGI 204
<i>E. coli</i> Atu4426	LDA--FRHL T LDG H CPGLGKELNAYITAGIENC HE SYQLEEGRRKLQ L GMSLMIREGSA 260 VQAGLAAEKLVCG H ARGLKNADLNAFMAAGVSSD HE LVSGEDLMAKLRAGLTIELR-GSH 263
<i>E. coli</i> Atu4426	ARNLNALAPLINEFNS-PQCM-LCT DD RN P WEIAHEGHIDALIRRLIEQHN V PLHVAYRV 318 DHLLEPFVAALNTLGHLPQ T VTLC TD VFPDDL L QGGGLDDV V RRLV-RYGLKPEWALRA 322
<i>E. coli</i> Atu4426	ASWSTARHFGLNHLG L LAPGKQADIVLLSDARKVTVQ V LVKGEPIDAQTLQAEESARLA 378 ATLNAAQRLGRSD L GLIAAGRRADIVVFEDLNGFSARHVLASGRAV-----AEGGRML 375
<i>E. coli</i> Atu4426	QSAPPYGN T IARQPVS-----ASDFALQFTPGKRYRVIDVIHNELITHSHSSVYSENGF- 432 VDIPTCD T TVLKGSMK L PLRMANDFLVK-SQGAKVRLATIDRPRFTQWGETEADV K DGFV 434
<i>E. coli</i> Atu4426	-DRDDVSFI AV LERYGQ-RLAPACGLLGGFGLNEGALAA T VS ED SHNIVVIGR S AEEMAL 490 VPPEGATMISV TH RHGMAEPTTKTGFLTGWGRWNGAFATT VS EDSHNLT V FGNAGDMAL 494
<i>E. coli</i> Atu4426	AVNQVIQDGGGLCVVRNGQVQSHLPLPIAGLMSTDTAQSLAEQIDALKAA 540 AANAVIGTGGGM AV ASEGKVTAILPLPLSGLVSDAPLEEVARAFEDLREA 544

binding of the third metal ion in the active site is not required for catalytic activity. Apparently, the third metal appears in the structure as a result of metal supplementation during bacterial growth and/or protein crystallography and plays no role in the deaminase reaction.

A sequence alignment of *E. coli* ADE and Atu4426 is presented in Scheme 2. The residues highlighted in yellow are direct ligands to the binuclear metal center. All of the other structurally characterized aromatic deaminases found within the amidohydrolase superfamily bind a single divalent cation in the active site (5). These deaminases bind a single divalent cation at the α -site and use a conserved HxxE motif from the end of β -strand 5 to deliver a proton to a ring nitrogen of the reaction product. The conserved aspartate at the end of β -strand 8 protonates the leaving group ammonia. The HxxE motif is absent from all of the adenine deaminases from cog1001, and thus, the details of the catalytic mechanism for ADE must be different from those for the other deaminases in the AHS. The residues highlighted in green represent the residues that are highly conserved in all the adenine deaminases in cog1001 and are close to the active site. These residues were mutated to determine their significance in catalytic activity.

On the basis of our model for the binding of adenine in the active site of ADE, we conclude that the invariant glutamate from the end of β -strand 6 functions to protonate N-1 of adenine during catalysis. In *E. coli*, this residue is Glu-236. This residue is part of the highly conserved HE motif found in all adenine deaminases in cog1001. We also conclude that Asp-284 in the *E. coli* protein is unprotonated and functions in catalysis by abstraction of the proton from the tetrahedral intermediate and subsequent delivery of this proton to the ammonia leaving group. Shown in Scheme 3 is our working model for the chemical mechanism for adenine deaminase from *E. coli*. In this scheme, a proton is transferred from the bridging water molecule to Glu-236. The bridging hydroxide attacks C-6 on the *re* face of adenine to form a tetrahedral intermediate with *R* stereochemistry, and the proton from Glu-236 is transferred to N-1 of the intermediate. Subsequently, the proton from the attacking hydroxide is transferred to Asp-284. The tetrahedral intermediate collapses, leading to the transfer of the proton from Asp-284 to ammonia.

Scheme 3



ACKNOWLEDGMENT

We thank Dr. Dao Feng Xiang (Texas A&M University) for cloning adenine deaminase from *E. coli*. We gratefully acknowledge data collection support from beamline X25 (National Synchrotron Light Source).

SUPPORTING INFORMATION AVAILABLE

Titration of apo-Atu4426 with Mn^{2+} and Fe^{2+} (Figure S1). This material is available free of charge via the Internet at <http://pubs.acs.org>.

REFERENCES

- Petersen, C., Moller, L. B., and Valentin-Hansen, P. (2002) The cryptic adenine deaminase gene from *Escherichia coli*. *J. Biol. Chem.* 277, 31373–31378.
- Matsui, H., Shimaoka, M., Kawasaki, H., Takenaka, Y., and Kurahashi, O. (2001) Adenine deaminase activity of the *yicP* gene product of *Escherichia coli*. *Biosci., Biotechnol., Biochem.* 65, 1112–1118.

- Oestricher, N., Ribard, C., and Scazzocchio, C. (2008) The *nadA* gene of *Aspergillus nidulans*, encoding adenine deaminase, is subject to a unique regulatory pattern. *Fungal Genet. Biol.* 45, 760–775.
- Holm, L., and Sander, C. (1997) An evolutionary treasure: Unification of a broad set of amidohydrolases related to urease. *Proteins: Struct., Funct., Genet.* 28, 72–82.
- Seibert, C. M., and Raushel, F. M. (2005) Structural and catalytic diversity within the amidohydrolase superfamily. *Biochemistry* 44, 6383–6391.
- Wang, Z., and Quincho, F. A. (1998) Complexes of adenosine deaminase with two potent inhibitors: X-ray structures in four independent molecules at pH of maximum activity. *Biochemistry* 37, 8314–8324.
- Wilson, D. K., Rudolph, F. B., and Quincho, F. A. (1991) Atomic structure of adenosine deaminase complexed with transition state analog: Understanding catalysis and immunodeficiency mutations. *Science* 252, 1278–1284.
- Benning, M. M., Shim, H., Raushel, F. M., and Holden, H. M. (2001) High resolution structures of different metal substituted forms of phosphotriesterase from *Pseudomonas diminuta*. *Biochemistry* 40, 2712–2722.
- Benning, M. M., Hong, S.-B., Raushel, F. M., and Holden, H. M. (2000) The binding of substrate analogs to phosphotriesterase. *J. Biol. Chem.* 275, 30556–30560.
- Jabri, E., Carr, M. B., Hausinger, R. P., and Karplus, P. A. (1995) The crystal structure of urease from *Klebsiella aerogenes*. *Science* 268, 998–1004.
- Thoden, J. B., Marti-Arbona, R., Raushel, F. M., and Holden, H. M. (2003) High-resolution X-ray structure of isoaspartyl dipeptidase from *Escherichia coli*. *Biochemistry* 42, 4874–4882.
- Marti-Arbona, R., Fresquet, V., Thoden, J. B., Davis, M. L., Holden, H. M., and Raushel, F. M. (2005) Mechanism of the reaction catalyzed by isoaspartyl dipeptidase from *Escherichia coli*. *Biochemistry* 44, 7115–7124.
- Pace, C. N., Vajdos, F., Fee, L., Grimsley, G., and Gray, T. (1995) How to measure and predict the molar absorption coefficient of a protein. *Protein Sci.* 4, 2411–2423.
- Hall, R. S., Xiang, D. F., Xu, C., and Raushel, F. M. (2007) N-Acetyl-D-glucosamine-6-phosphate deacetylase: Substrate activation via a single divalent metal ion. *Biochemistry* 46, 7942–7952.
- Muszbeck, L., Polgar, J., and Fesus, L. (1985) Kinetic determination of blood coagulation factor XIII in plasma. *Clin. Chem.* 31, 35–40.
- Otwinowski, Z., and Minor, W. (1997) Processing of X-ray diffraction data collected in oscillation mode. *Methods Enzymol.* 276, 307–326.
- Schneider, T. R., and Sheldrick, G. M. (2002) Substructure solution with SHELXD. *Acta Crystallogr. D* 58, 1772–1779.
- De La Fortelle, E. (1997) Maximum-likelihood heavy atom parameter refinement in the MIR and MAD methods. *Methods Enzymol.* 276, 472–493.
- Abrahams, J. P., and Leslie, A. G. (1996) Methods used in the structure determination of bovine mitochondrial F1 ATPase. *Acta Crystallogr. D* 52, 30–42.
- Langer, G., Cohen, S. X., Lamzin, V. S., and Perrakis, A. (2008) Automated macromolecular model building for X-ray crystallography using ARP/wARP version 7. *Nat. Protoc.* 3, 1171–1179.
- Emsley, P., and Cowtan, K. (2004) Coot: Model-building tools for molecular graphics. *Acta Crystallogr. D* 60, 2126–2132.
- Murshudov, G. N., Vagin, A. A., and Dodson, E. J. (1997) Refinement of macromolecular structures by the maximum-likelihood method. *Acta Crystallogr. D* 53, 240–255.
- Lin, D., Manning, N. O., Jiang, J., Abola, E. E., Stampf, D., Prilusky, J., and Sussman, J. L. (2000) AutoDep: A web-based system for deposition and validation of macromolecular structural information. *Acta Crystallogr. D* 56, 828–841.
- Sali, A., and Blundell, T. L. (1993) Comparative protein modeling by satisfaction of spatial restraints. *J. Mol. Biol.* 234, 779–815.
- Sherman, W., Day, T., Jacobson, M. P., Freisner, R. A., and Farid, R. (2006) Novel procedure for modeling ligand/receptor induced fit effects. *J. Med. Chem.* 49, 534–553.
- Hermann, J. C., Ghanem, E., Li, Y. C., Raushel, F. M., Irwin, J. J., and Shoichet, B. K. (2006) Predicting substrates by docking high-energy intermediates to enzyme structures. *J. Am. Chem. Soc.* 128, 15882–15891.
- Hermann, J. C., Marti-Arbona, R., Fedorov, A. A., Fedorov, E., Almo, S. C., Shoichet, B. K., and Raushel, F. M. (2007) Structure-based activity prediction for an enzyme of unknown function. *Nature* 448, 775–780.
- Kanehisa, M., and Goto, S. (2000) KEGG: Kyoto of genes and genomes. *Nucleic Acids Res.* 28, 27–30.
- Lorber, D. M., and Shoichet, B. K. (2005) Hierarchical docking of databases of multiple ligand conformations. *Curr. Top. Med. Chem.* 5, 739–749.
- Meng, E. C., Shoichet, B. K., and Kuntz, I. D. (1992) Automated docking with grid-based energy evaluation. *J. Comput. Chem.* 13, 505–524.
- Chenlo, F., Moreira, R., Pereira, G., and Ampudia, A. (2002) Viscosities of aqueous solutions of sucrose and sodium chloride of interest in osmotic dehydration processes. *J. Food Eng.* 54, 347–352.
- Morrison, J. F. (1969) Kinetics of the reversible inhibition of enzyme-catalysed reactions by tight-binding inhibitors. *Biochim. Biophys. Acta* 185, 269–286.
- Shim, H., and Raushel, F. M. (2000) Self-assembly of the binuclear metal center of phosphotriesterase. *Biochemistry* 39, 7357–7364.
- Dewitt, J. G., Bentsen, J. G., Rozenweig, A. C., Hedman, B., Green, J., Pilkington, S., Papaefthymiou, G. C., Dalton, H., Hodgson, K. O., and Lippard, S. J. (1991) X-ray absorption, Mössbauer and EPR studies of the dinuclear iron center in the hydroxylase component of methane monooxygenase. *J. Am. Chem. Soc.* 113, 9219–9235.
- Thomann, H., Bernardo, M., McCormick, J. M., Pulver, S., Andersson, K. K., Lipscomb, J. D., and Solomon, E. I. (1993) Pulsed EPR studies on the mixed valent [Fe(II)Fe(III)] forms of hemerythrin and methane monooxygenase: Evidence for a hydroxide bridge. *J. Am. Chem. Soc.* 115, 8881–8882.
- Kurtz, D. M., Jr. (2006) Avoiding high-valent iron intermediates: Superoxide reductase and ruberythrin. *J. Inorg. Biochem.* 100, 679–693.
- Weiss, P. M., Cook, P. F., Hermes, J. D., and Cleland, W. W. (1987) Evidence from nitrogen-15 and solvent deuterium isotope effects on the chemical mechanism of adenosine deaminase. *Biochemistry* 26, 7378–7384.
- Cleland, W. W. (1992) Low-barrier hydrogen bonds and low fractionation factor bases in enzymatic reactions. *Biochemistry* 31, 317–319.
- Merkler, D. J., and Schramm, V. L. (1993) Catalytic mechanism of yeast adenosine 5'-monophosphate deaminase. Zinc content, substrate specificity, pH studies, and solvent isotope effects. *Biochemistry* 32, 5792–5799.